AD-A040 346 CHEMICAL SYSTEMS LAB (ARMY) ABERDEEN PROVING GROUND MD F/G 6/17
NONDESTRUCTIVE TESTING OF STRUCTURAL DEFICIENCIES IN PROTECTIVE--ETC(U)
MAY 77 P D DIXON

UNCLASSIFIED ARCSL-TR-77022 EP-TR-77028 NL

| OF |
AD
A040 346

END

DATE
FILMED
6-77

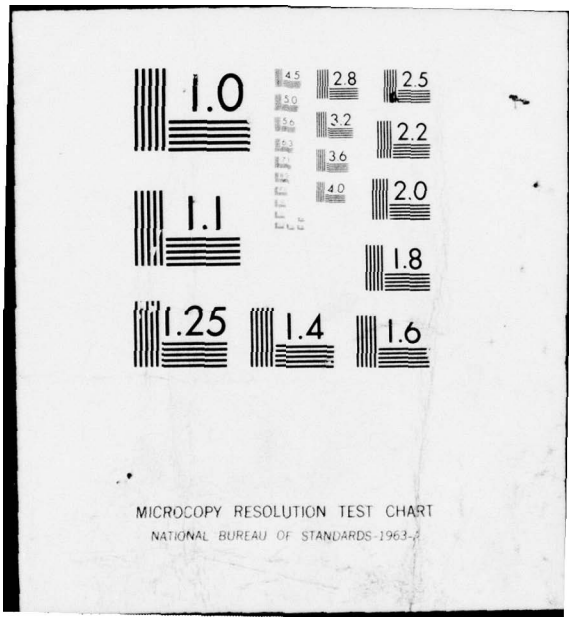
1.0
4.5
5.0
5.6
6.3
7.1
2.8
3.2
3.6
4.0
2.5
2.2
2.0
1.8
1.1
1.25
1.4
1.6
MICROCOPY RESOLUTION TEST CHART
NATIONAL BUREAU OF STANDARDS-1963-A

(12)

AD

TECHNICAL REPORT ARCSL-TR-77022
(EP-TR-77028)

NONDESTRUCTIVE TESTING OF STRUCTURAL DEFICIENCIES IN PROTECTIVE FILTERS

by

Ponce D. Dixon

Chemical Systems Division
Product Assurance Directorate

May 1977

DEPARTMENT OF THE ARMY
US Army Armament Research and Development Command
Chemical Systems Laboratory
Aberdeen Proving Ground, Maryland 21010

Approved for public release; distribution unlimited.

Disclaimer

The findings in this report are not to be construed as an official Department of the Army position unless so designated by other authorized documents.

Disposition

Destroy this report when it is no longer needed. Do not return it to the originator.

UNCLASSIFIED

SECURITY CLASSIFICATION OF THIS PAGE (When Data Entered)

REPORT DOCUMENTATION PAGE

READ INSTRUCTIONS BEFORE COMPLETING FORM

1. REPORT NUMBER: ARCSL-TR-77022	2. GOVT ACCESSION NO.
3. RECIPIENT'S CATALOG NUMBER	
4. TITLE (and Subtitle): NONDESTRUCTIVE TESTING OF STRUCTURAL DEFICIENCIES IN PROTECTIVE FILTERS	5. TYPE OF REPORT & PERIOD COVERED: Technical Report July 1973–July 1976
6. PERFORMING ORG. REPORT NUMBER: EP-TR-77028	
7. AUTHOR(s): Ponce D. Dixon	8. CONTRACT OR GRANT NUMBER(s)
9. PERFORMING ORGANIZATION NAME AND ADDRESS: Commander, ARRADCOM, Attn: DRDAR-QAC-E, Aberdeen Proving Ground, Maryland 21010	10. PROGRAM ELEMENT, PROJECT, TASK AREA & WORK UNIT NUMBERS: Project MTT 5741291
11. CONTROLLING OFFICE NAME AND ADDRESS: Director, Chemical Systems Laboratory, Attn: DRDAR-CLJ-I, Aberdeen Proving Ground, Maryland 21010	12. REPORT DATE: May 1977 13. NUMBER OF PAGES: 33
14. MONITORING AGENCY NAME & ADDRESS (if different from Controlling Office): Army Materials & Mechanics Research Center, Attn: AMXMR-QA, Watertown, Massachusetts 02172	15. SECURITY CLASS. (of this report): UNCLASSIFIED 15a. DECLASSIFICATION/DOWNGRADING SCHEDULE: NA

16. DISTRIBUTION STATEMENT (of this Report)

Approved for public release; distribution unlimited.

17. DISTRIBUTION STATEMENT (of the abstract entered in Block 20, if different from Report)

18. SUPPLEMENTARY NOTES

19. KEY WORDS (Continue on reverse side if necessary and identify by block number)

Protective filters
Edgeseal attenuation
Thermal imaging
Charcoal padding
Nondestructive testing
Plasticizer
Radiation

20. ABSTRACT (Continue on reverse side if necessary and identify by block number)

This report describes adaptations of nondestructive testing methods used for detecting defects in protective filter elements. Thermal imaging revealed some flaws in the plasticizer material used for sealing the charcoal impregnated filtration pads and in other areas of the filter.

Radiation gauging and X-ray vidicon proved successful for inspecting filters by real-time scanning. These processes obviated the human element and were conducive to assembly-line-type production. Low kilovolt manual X-radiography proved invaluable in refining the other techniques used in this study, all of which hold promise for accelerated inspection.

DD FORM 1 JAN 73 1473 EDITION OF 1 NOV 65 IS OBSOLETE

UNCLASSIFIED

SECURITY CLASSIFICATION OF THIS PAGE (When Data Entered)

PREFACE

The work described in this report was authorized under Project MTT 5741291, Development of Nondestructive Testing Methods for Structural Deficiencies in Protective Filters. The work was started in July 1973 and completed in July 1976.

The use of trade names in this report does not constitute an official endorsement or approval of the use of such commercial hardware or software. This report may not be cited for purposes of advertisement.

Acknowledgment

The author wishes to acknowledge the technical assistance of Kenneth W. Earnhardt, Edgewood Arsenal, and Robert McClung, W. A. Simpson, Jr., and B. E. Foster, Oak Ridge National Laboratory, for their work on this project.

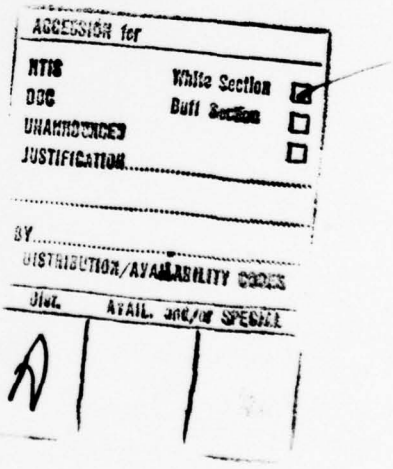

SUMMARY

Many protective filters used for personnel protection against lethal airborne chemical agents contain structural flaws that usually are not detected by laboratory performance tests. These flaws constitute a weakened structure which can eventually result in performance failures especially after being subjected to stresses not normally encountered in laboratory testing, packaging, and shipping. Most of these hidden defects can be detected by classical radiography, but prohibitive costs and time preclude the effective use of manual radiography.

Infrared techniques have been successfully applied for detecting several types of defects in protective filters. Other techniques employed with some degree of success were X-ray sensitive vidicon and radiation gauging, both of which are advances from the outgrowth of classical radiography.

CONTENTS

LIST OF FIGURES

LIST OF FIGURES (Contd)

NONDESTRUCTIVE TESTING OF STRUCTURAL DEFICIENCIES IN PROTECTIVE FILTERS

I. INTRODUCTION.

Protective filter elements are critical components of equipment designed to provide individual defense against lethal airborne chemicals. Any filtration system is no better than the overall performance of its filtering element. By nature of their design, protective filter elements are not readily adapted to rapid nondestructive testing by classical methods. Many internal defects are subtle and can barely be discerned. This study involves the investigation of characteristics considered inspectable by nondestructive testing (NDT) approaches. Primary efforts were directed toward infrared and radiographic techniques.

II. INSPECTION APPROACH.

A. Requirements.

Previously, the inspection of filter elements was primarily destructive in nature or was conducted by visual observation of defects which were manifested by surface indications. Certain functionability tests, such as a measurement of airflow capacity and the time-to-failure of the neutralizing medium, were also conducted, but they do not give a reasonably good indication of the filter's structural integrity.

Current design requires fabrication using a variety of polymeric materials which have similar thermal, electrical, and physical properties. The location and orientation of critical junctions make most routine NDT methods ineffective. There exists the need for automated inspection techniques amenable to high volume production at low cost.

B. Filter Types and Defects.

In considering means of nondestructively testing protective filters, two types of filters were selected for study. One is the M13A2 filter element for the M17 protective mask, and the other is the M2 filter pad element for the infant protector enclosure. These filters differ in size and design but are fabricated from similar material. To a great extent, the same types of defects are common to both types of filters. The infant protector filter, shown in figure 1, is rectangular with a perimeter of approximately 56 inches, with a maximum thickness of 1/3 inch in the border. The large surface area of this filter panel facilitates the exchange of air at low pressures conducive to infant breathing.

Nearly all of the defects in the filter panel occur in the edgeseal area where charcoal-impregnated pads are bound by a plasticized compound called edgeseal which solidifies under heat and pressure to form a rigid border. Figure 2 shows a cutaway view of the M2 panel.

Voids, comprised of cracks, porosity, blisters, and open channels are the most frequently occurring defects in this filter. They may significantly weaken the filter's structure as well as present an incipient path bypassing the neutralizing element of the filter. Figure 2 shows an open-channel-type void in the edgeseal. Voids comprise one of the more serious, subtle defects and they cannot usually be detected by visual inspection. In some cases, wherein voids extend close to the surface, they can be detected visually by flexing the edgeseal while watching for bubble-like appearances.

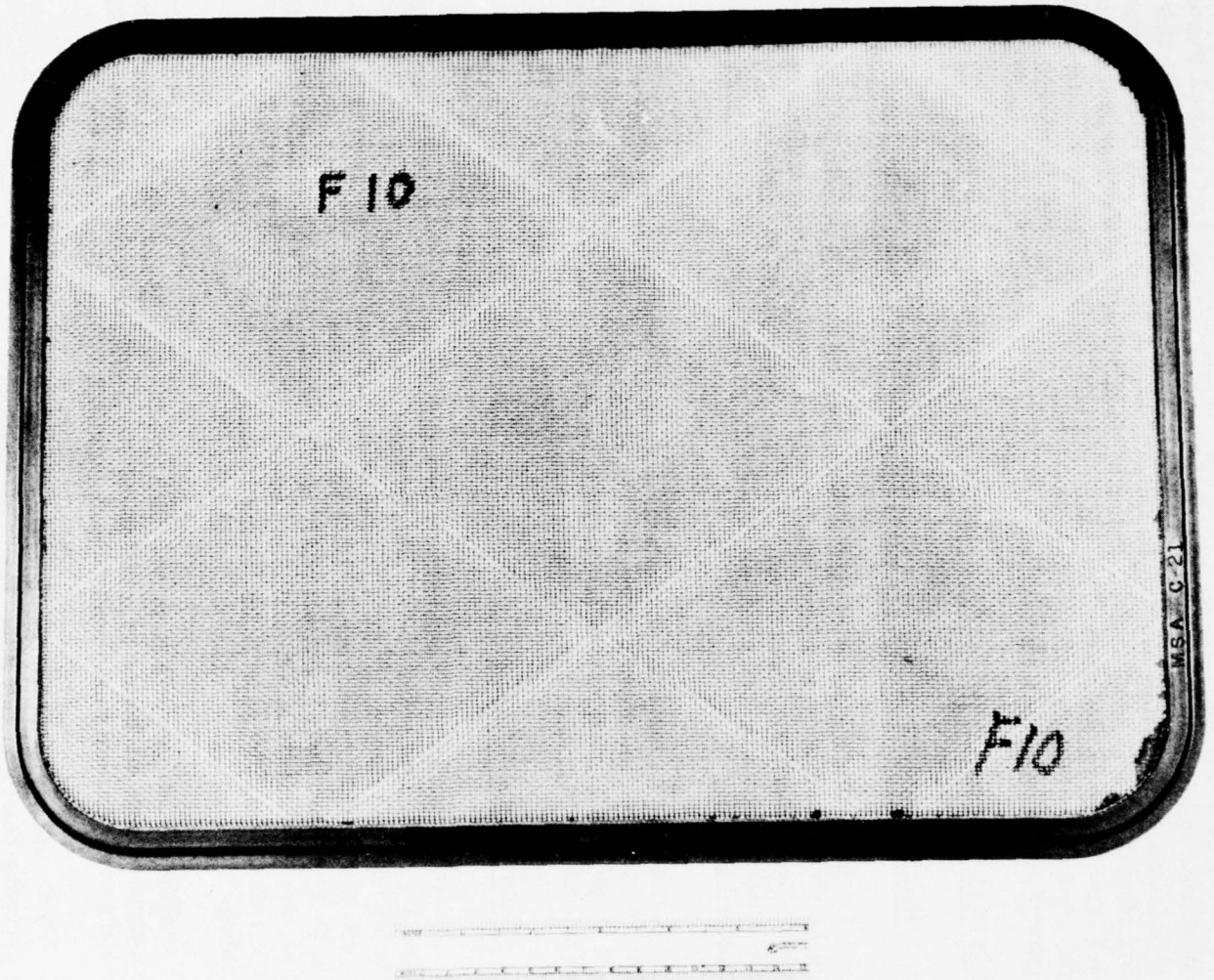

Figure 1. Filter Panel for M2 Infant Protector

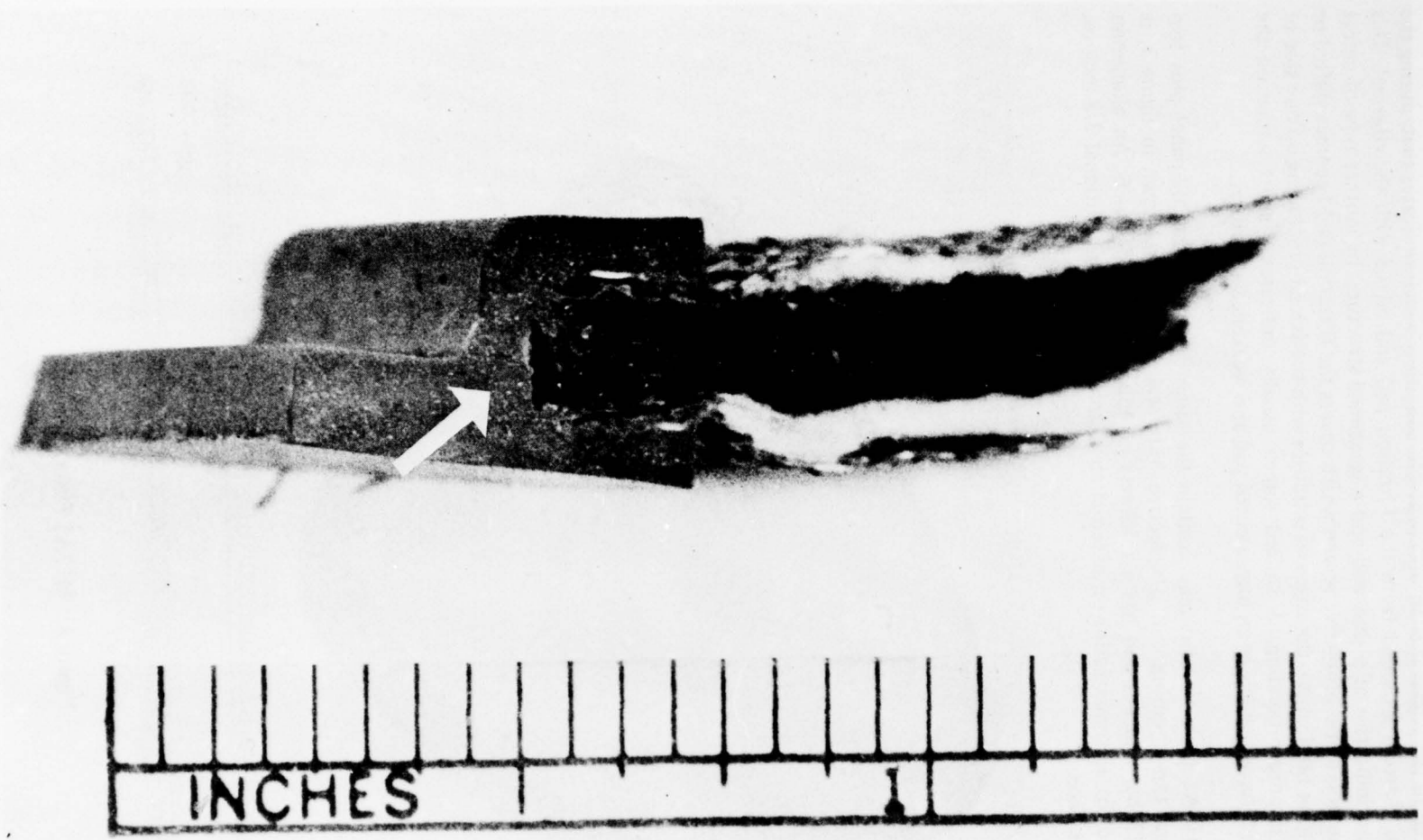

Figure 2. Section of M2 Filter Panel Showing Open Channel Void

Charcoal in the edgeseal is an unacceptable condition which indicates that, during the fabrication process, charcoal loosened from the filtration pad and mixed with the edgeseal. This type of defect is also indicative of a thin wall and a weakened structure. In another type of defect called screening, the polymeric protective screen which covers the filtration pad becomes shifted or is unevenly cut. During fabrication, the edgeseal solidifies with the screen protruding on one side of the panel causing improper bonding. A shifted screen usually indicates a short screen on the opposite side of the filter which leaves an unprotected pad and weakened structure.

The M13A2 filter element may contain the same defects as the M2 panel plus two additional significant types: coring and a defective butt seal. This filter, shown in figure 3, is approximately 5-1/2 by 4 inches and has a thickness of approximately 3/4 inch. An aluminum connector ring, used for accommodating an external air source, extends an additional 3/8 inch on the filter's convex surface.

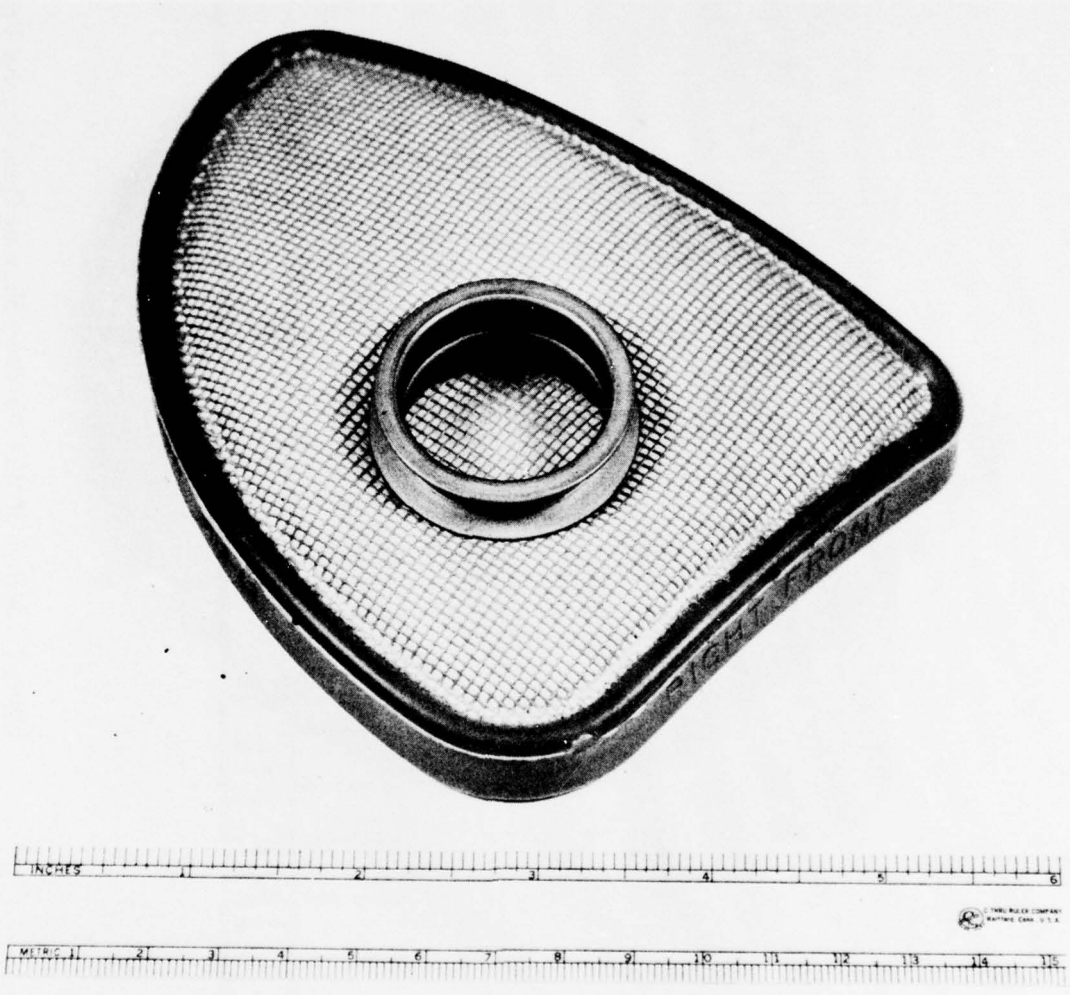

Figure 3. M13A2 Filter Element

The displaced screen mentioned above which is common to both types of filters is shown in figure 4. Screening is more prevalent in the M13A2, probably because of this filter's more complex design. This defect can frequently be detected by visual inspection.

Coring is a hard-to-detect flaw directly beneath the connector ring. It is believed to originate during the fabrication process when the connector is crimped securely to the filtration pad and polypropylene stifferator. The filtration pad is sheared in an arc susceptible to forming an annulus around the connector thus forming a channel partly bypassing the filtration pad. Coring in the assembled filter has not been successfully detected by gamma-, neutron-, or X-radiography.

The defective butt seal can originate from a variety of causes such as a shifted pad, improper mold temperature, dirty or dusty padding. This defect causes a weakened structure in the edgeseal area and often results in a thin wall, a void, or a separation of the filtration pads. Unless severe, a defective butt seal cannot be detected visually without sectionalizing the filter. Figure 5 shows a defective butt seal.

Other defects occur in both the M2 filter panel and the M13A2 filter element but are not considered as detrimental as those already mentioned, primarily because of the infrequency of occurrence or because they would be readily recognized at some station during fabrication.

C. Inspection Techniques.

Thermal Method. The thermal technique considered feasible for this study involved the use of an infrared imaging system. The specimen being tested must undergo a temperature change in order to enhance defect detection. The primary method employed was dynamic heating which consisted of rapidly heating the specimen's surface by convection currents. Theoretically, internal flaws absorb heat at a different rate than the surrounding area forming an isotherm which is then detected by an infrared sensitive camera.

Two important factors which help determine the applicability of thermal testing techniques are the rate of introduction or absorption of heat (thermal gradient) of a specimen and the time frame in which the thermal contrast between the specimen and defect is at a maximum. Generally, in thermal testing, a defect is only detectable if its depth beneath the surface is less than or equal to its diameter or minor dimension. Also, if the defect is an inclusion whose thermal impedance approaches that of the host material, detectability will be reduced.

Initially, the Oak Ridge National Laboratory (ORNL) approached the investigation using computer modeling. Necessary thermal characteristics of the edgeseal material were adopted using values of soft rubber whose physical properties approximated those of the edgeseal, these being thermal conductivity, 1.28×10^{-4} Btu/in min °F. and specific heat, 0.45 Btu/lb °F. The measured density of the edgeseal was 4.66×10^{-2} lb/in^3.

In determining heat input rate and time of maximum thermal contrast, the function may be resolved into its Fourier components and each harmonic treated separately. The velocity of a harmonic thermal wave propagating through a material is given by the equation $V = \sqrt{2\,kw}$,* where k is the diffusivity of the material and w the angular frequency of the wave. The wave is attenuated as $e^{-2\pi x/\lambda}$, where x is the distance into the material and λ the wavelength. The factors w and λ are related by $w = 8\pi^2\ k/\lambda^2$. This indicates that thermal waves are attenuated in proportion to their frequency and that the time of optimum thermal contrast of a flaw can be calculated.

*Carslaw, H. S., and Jaeger, J. C. Conduction of Heat in Solids. 2d Ed. p 66. Clarendon Press, Oxford, England. 1959.

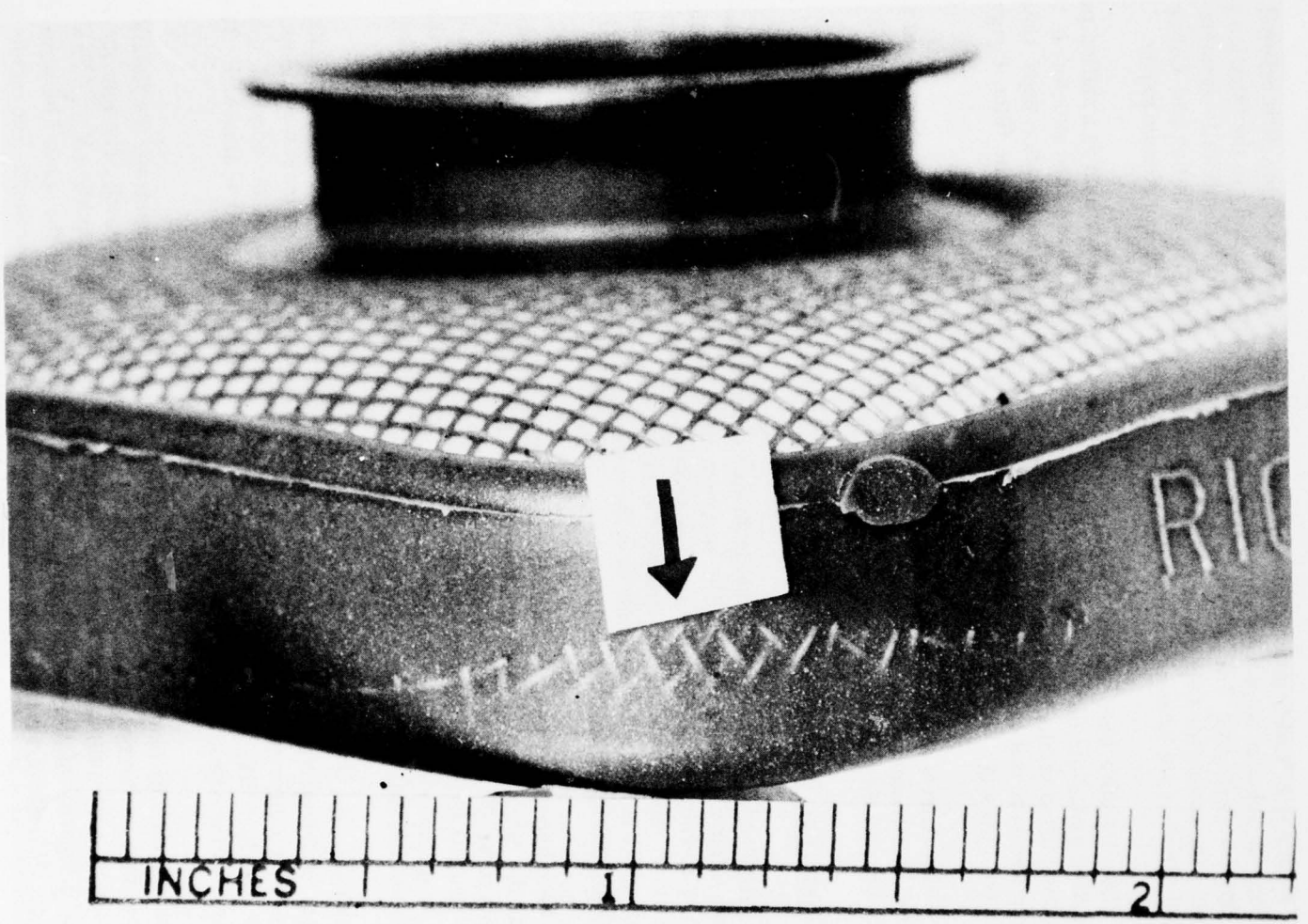

Figure 4. Displaced Screen Defect in M13A2 Filter

Figure 5. Defective Butt Seal

When heat is first applied to a specimen, the shorter wavelengths travel quickly but are damped out in a short distance; but, as time progresses, the longer waves propagate to greater depths into the material. The earliest detection time of a subsurface flaw occurs when a wavelength equal to the depth of the defect has reached the defect and reflected back to the surface. Shorter waves are severely attenuated and longer ones, having slower velocities, take longer to be reflected.

For experimental tests, a slab of edgeseal material measuring 4-5/6 by 3-1/8 by 0.48 inch was prepared by drilling two flat-bottomed holes inwardly from the back surface. These simulated defects measured 5/16 inch and 5/32 inch in diameter and both were drilled to within 5/32 inch of the front furface. The smaller hole's depth was equal to its diameter and should be marginally detectable.

A thermal wave with λ=5/32 inch propagates through the edgeseal at a velocity of 0.49 inch per minute and takes approximately 38 seconds to travel to the flaw and back. This is the earliest time after initial heating that one can expect to detect the flaw using an infrared camera. Assuming total reflection, the amplitude of that wave is attenuated to approximately 0.0003% of its original value. The longer (and slower) waves are attenuated less, but as λ exceeds the size of the defect the coefficient of reflection decreases thus lowering the resolution of the thermal waves.

For a defect 5/32 inch in diameter, with the same depth, the maximum contrast in detecting infrared radiation occurs when wavelengths of two or three times the defect diameter are reflected to the surface. The times involved are 1.27 minutes and 1.92 minutes, respectively.

Penetrating Ionizing Radiation. All materials are permeable to penetrating ionizing radiation. Each material has a characteristic interaction with the radiation being projected through it. By analyzing the exiting beam for such qualities as degree of attenuation, the physical integrity of that material can be determined. Three adaptations of the use of penetrating ionizing radiation for examining protective filters are given below:

1. Low Kilovolt X-Ray (Manual). Since all of the material used in the fabrication of both types of filters has low density values, low kilovolt X-ray should be optimally suited for routine radiographic applications. All of the NDT techniques for inspecting subsurface defects can be supplemented by manual X-ray initially, because this well-established process is invaluable in locating and providing a permanent visual record of deficiencies.

Factors, which preclude the use of manual radiography in high volume production and particularly in the case of protective filter elements, are excessive costs and time required to produce a radiograph.

2. X-Ray Sensitive Vidicon. A method of scanning considered applicable for inspecting filter elements is the X-ray-sensitive vidicon. The equipment used was a Cohu black and white closed-circuit television system with a Circon shading amplifier coupling the camera and monitor. The X-ray-sensitive camera was a Machlett Dynamicon type ML-589. A device for moving the filter for scanning was constructed from a series of pulleys and wire attached to a variable-speed motor.

A radiograph of a defective filter was used to establish optimum parameters of X-ray energy, current, focal distances, etc. The vidicon provides direct real-time static or in-motion viewing of most items which are normally viewed statically by radiograph. The system can be programmed to provide electronic rejection of defective items.

3. Radiation Gauging. This NDT technique involves real-time monitoring of the attenuated radiation as affected by flaws in the beam's path. Basic components of the gauging system consist of a radiation source, a detector, and a readout device or signal analyzer as shown in figure 6.

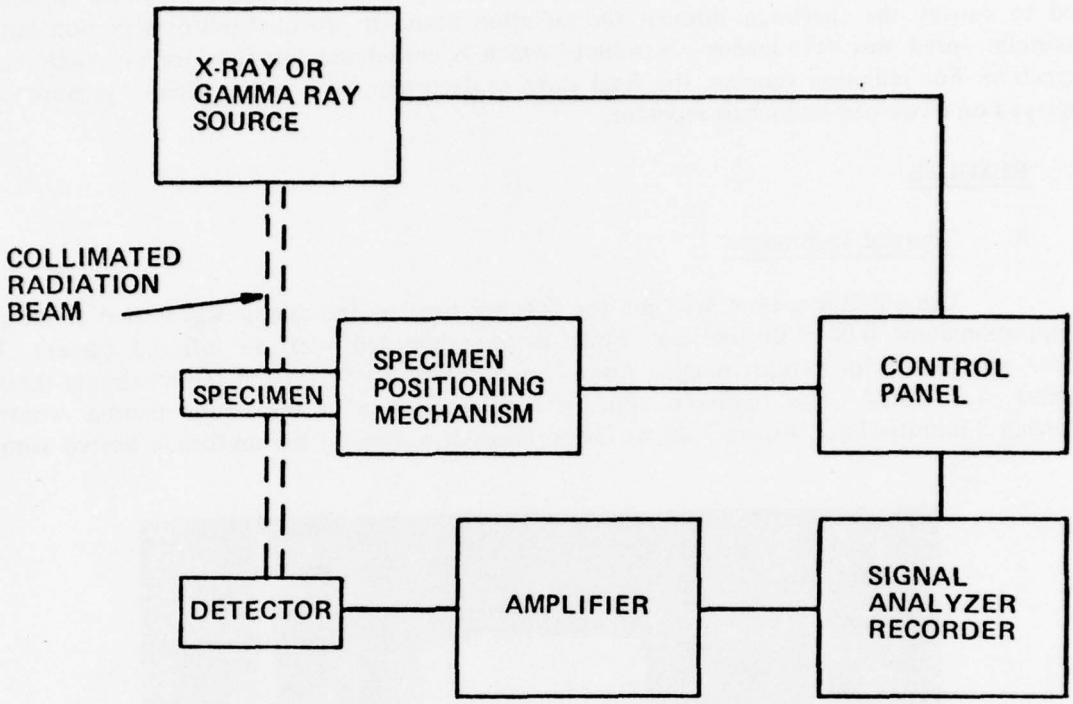

Figure 6. Block Diagram of Radiation Gauging System

In order to attain optimum sensitivity in gauging, the type and energy of radiation must be selected to match the mass attenuation coefficient of the edgeseal material. The applied cathode potential best suited for inspecting approximately 1/3 inch of edgeseal, as found in the M2 protective panel, is approximately 50 to 70 kv. At this potential, most of the radiation in the beam has an energy range of approximately 20 to 35 kv.

In this study, the X-ray equipment used did not provide the desired stable output of radiation. Therefore the use of this generator in radiation gauging was abandoned in favor of radioisotopes.

A gamma-emitting isotope, americium-241, was obtained for use as a source. It provided a stable output, but the 60-kv monoenergetic gamma ray proved to be only marginally effective for use with the edgeseal.

Another gamma emitter, iodine-125, was selected because of its 35-kv monoenergetic radiation. This isotope appeared to be ideal for inspecting protective filter elements using radiation gauging. The primary disadvantage of iodine-125 is its short, 60-day halflife.

A strontium-yttrium-90 isotope was also used as a source. This isotope emits 2.2-Mev beta radiation (high-speed electrons) which can penetrate approximately 1/2 inch of edgeseal material.

Radiation detectors used in this study were NaI(T1) and CaF_2(Eu) scintillating crystals, both types coupled with photomultiplier devices. A worm-gear-driven meter mover was used to convey the specimen through the radiation beam. It provided uniform motion but its maximum speed was 4.75 inches per minute which is considered too slow for production-type inspection. For radiation gauging, the final stage in detecting flaws in the filters was graphically displayed on a two-pen strip-chart recorder.

III. RESULTS.

A. Thermal Techniques.

Using a blower-type heat gun for dynamic heating, the sample was heated at the rate of approximately 0.0019 Btu/in^2 min while being monitored with an infrared camera. The surface was heated for periods ranging from 15 seconds to 2 minutes and the maximum thermal contrast was noted. The optimum time was 45 seconds with maximum thermal contrast occurring 2 minutes later. Figure 7 shows the rectangular outline of the uniformly heated sample.

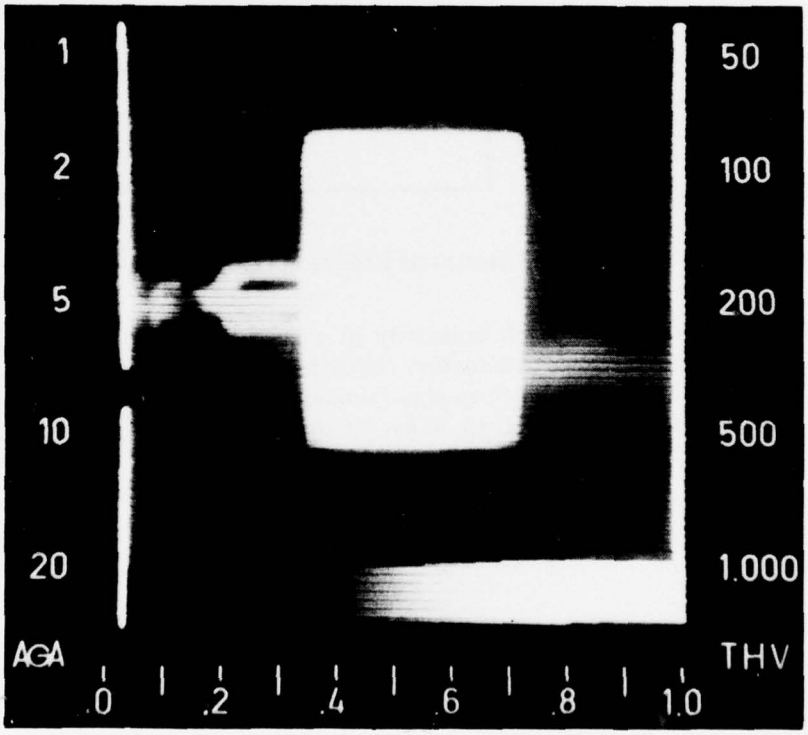

Figure 7. Thermal Profile of Uniformly Heated Sample

Figure 8 depicts the detection of the two holes 2 minutes after the cessation of heating. The bright spot on the left is the 5/16-inch-diameter hole; and that on the right, the 5/32-inch hole.

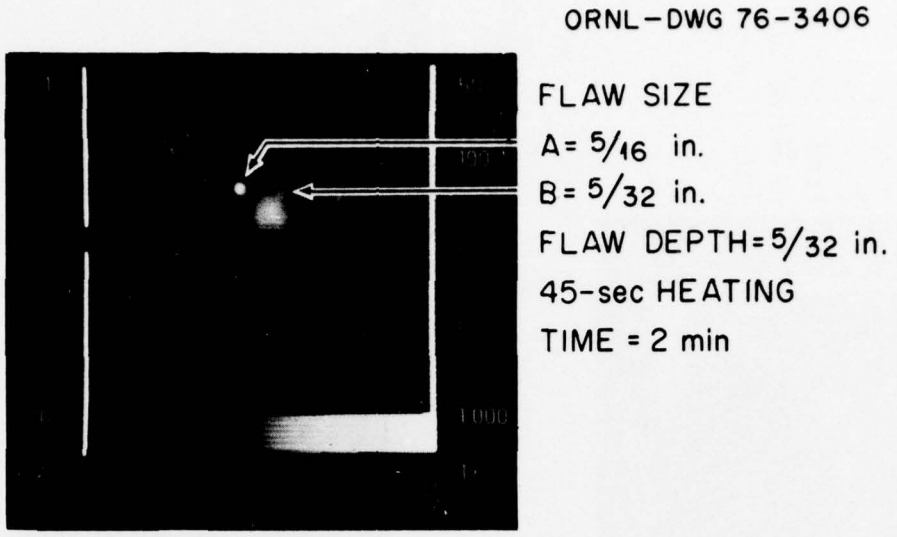

Figure 8. Sample, 2 Minutes After Heating

The surface temperature distribution at 1, 1.5, 2.5, and 3 minutes is shown in figure 9. Note that the smaller (right-hand) flaw is only marginally hotter (brighter) than the surrounding area, whereas the larger flaw is easily detected. Even at 3 minutes, the larger flaw is easily visible, though lateral diffusion has smeared its image, while the smaller flaw is barely detectable. This clearly indicated that voids could be detected down to a depth equal to their diameters in the edgeseal material, which is approximately the best that one could hope for in thermal testing. Though the simulated flaws were relatively large, this was for convenience rather than out of necessity.

Thermal Leakage. The M13A2 filters were also tested by blowing hot air into the filter while examining the input side with the infrared camera. Figure 10 shows the distribution for this type of filter. Note the approximately radial flow of heat along fairly-well-defined paths. These paths correspond roughly with channels in the white plastic separator in each filter as determined by sectioning this type of filter. Portions of the test apparatus used for holding the filter register as the two smaller light areas toward the top of the picture.

The heating element was turned off next and the test continued. Under these conditions, the temperature of the inlet air dropped rapidly and cooled the hot filter element. The temperature distribution of the filter under this cooling mode is shown in figure 11. Note that this distribution is now a thermal negative of figure 10 with the former hot spots now appearing cooler than the surrounding areas.

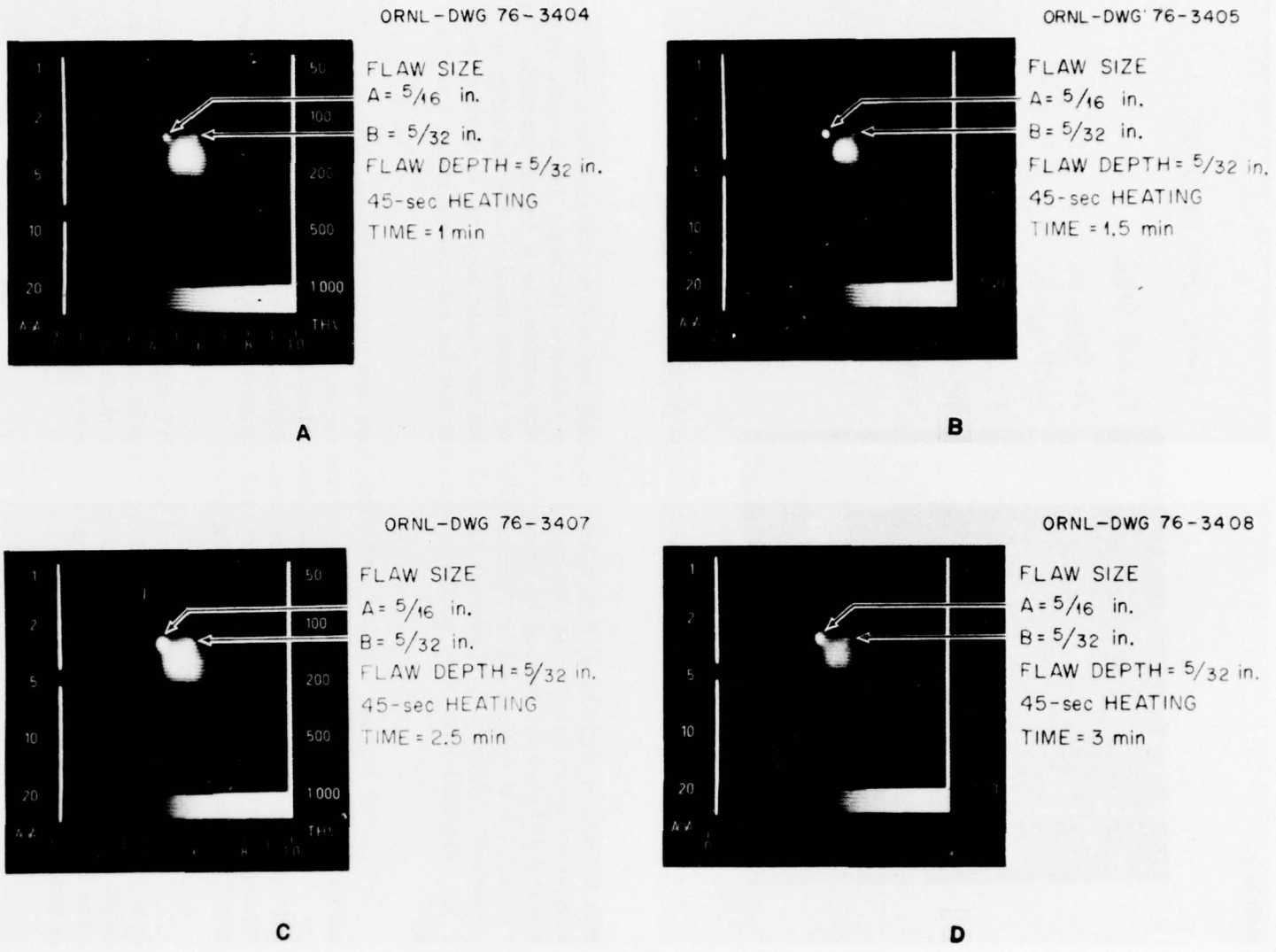

Figure 9. Surface Temperature Distribution of Sample at 1, 1.5, 2.5, and 3 Minutes

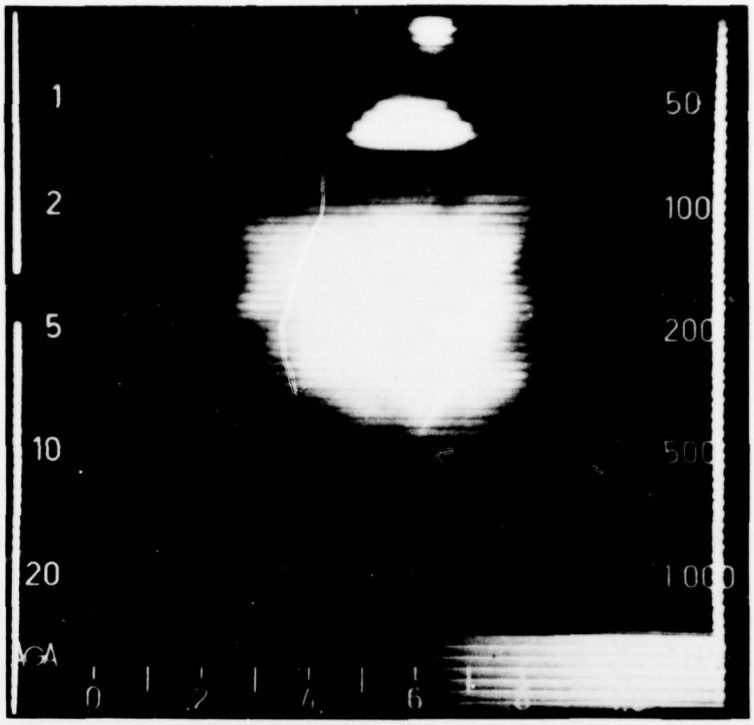

Figure 10. Infrared Distribution of Heat Flow from Normal M13A2 Filter

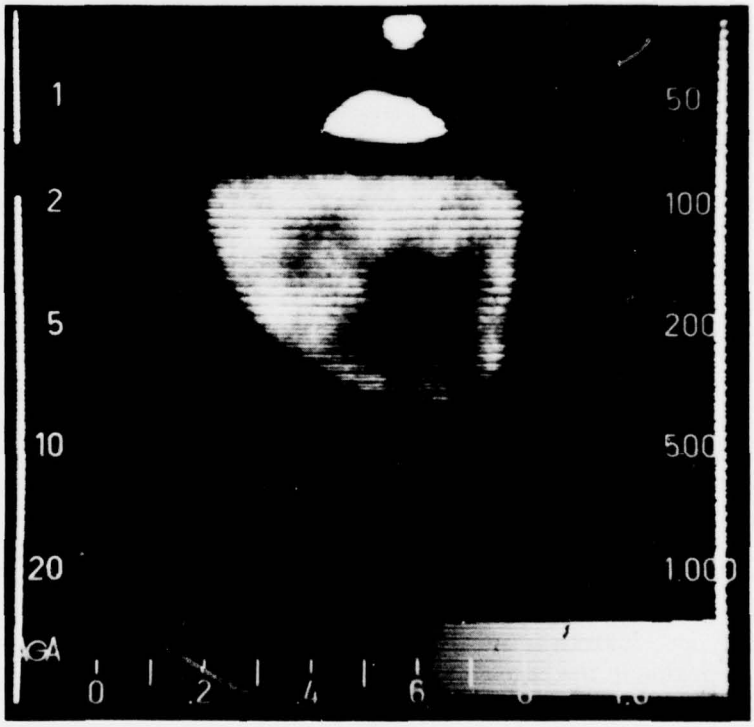

Figure 11. Inverse Thermal Effect of Heated Filter Being Cooled

Since no obvious leaks were detected in any of the filters, simulated ones were made by piercing the filter with hypodermic needles. Four holes were placed in filter No. D-3 with a needle 0.030 inch in diameter. The holes appeared to close when the needle was withdrawn and were quite difficult to locate visually. They were easily found by heating, however, as can be seen in figure 12. The four bright spots are caused by hot air streaming under pressure from the punctures.

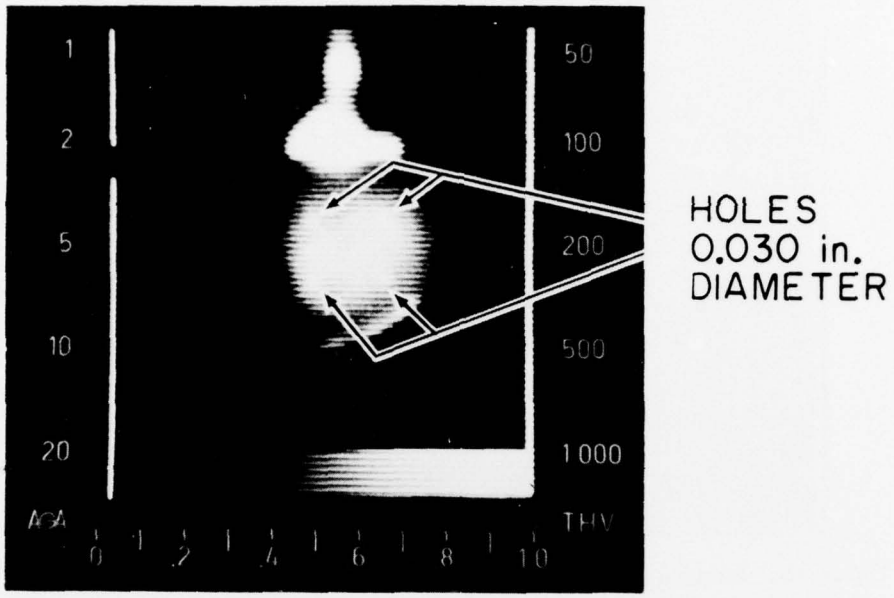

Figure 12. Thermal Image of Heated Air Leaking from 0.030-Inch Simulated Defects in Filter

Four additional holes having a diameter of 0.015 inch were then placed in filter No. D-3 in an octagonal arrangement with respect to the original four holes. The new punctures were completely undetectable visually. The thermal distribution is shown in figure 13. One of the smaller holes (below and between the lower two of the original four holes) is easily seen, whereas two are very faintly visible. In general, it was found that the 0.030-inch holes could always be detected while the 0.015-inch holes were sometimes detectable and sometimes not, depending upon their location. It appears that this technique can be useful for examining the entire filter for evidence of leakage and under conditions which approximate actual use.

This technique was also tried on one sample filter wherein coring was thought to be present. The area around the connector was monitored for thermal leakage which could emanate from a possible defect there. Coring was not detected. Subsequent sectioning of this filter revealed that coring was present although it could not be detected even by radiographic methods prior to disassembly.

B. Low-Kilovolt X-Ray.

Classical low kilovolt manual X-radiography proved to be excellent for detecting porosity, holes, or cracking in the edgeseal of the infant protector filter but only fair for detection of thin walls on the M13A2 filter. However, the limited investigation at Oak Ridge National Laboratory did not show screening, charcoal in the edgeseal, or short screens.

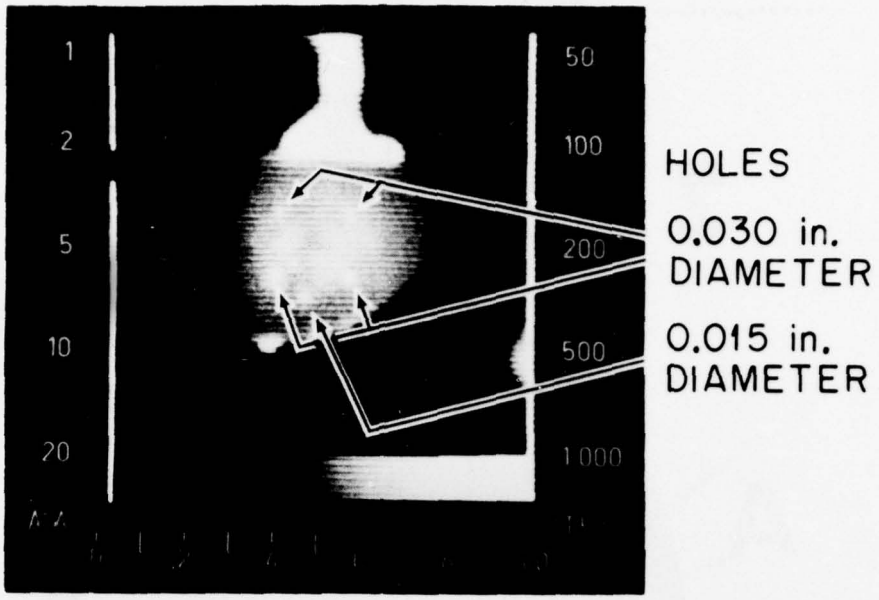

Figure 13. Thermal Image of Leakage from 0.030-Inch and 0.015-Inch Simulated Defects

Radiographic parameters were as follows:

1. Intensifying screens – no front screen and 0.010-inch-thick Pb back screen.

2. Type "M" X-ray film.

3. Exposure – 80 to 100 milliampere minutes.

4. Energy – 20 to 40 kilovolt constant potential

5. Film-to-focal distance – 65 inches.

6. Processing – manual according to manufacturer's recommendation. Figure 14 shows some of the defects which can be routinely detected with low kilovolt X-radiography.

Four sections (A, B, C, and D) of the edgeseal were removed by slicing through representative discontinuities, as seen in the prints of the radiograph. These sections are shown in figure 14 where the arrows in this figure denote the sample surfaces shown in figure 15.

Sample A is sliced through an area exhibiting a very sharp, jagged, cracklike indication on the radiograph. Note that the crack approaches 50% of the edgeseal thickness. Sample B is through an area showing a less sharp but wider indication than noted in sample A. Note the laminar- and linear-type void parallel to the X-ray beam direction. In sample C, an even wider indication than noted in sample B can be seen. Note the larger magnitude of the void area as well as the large pore.

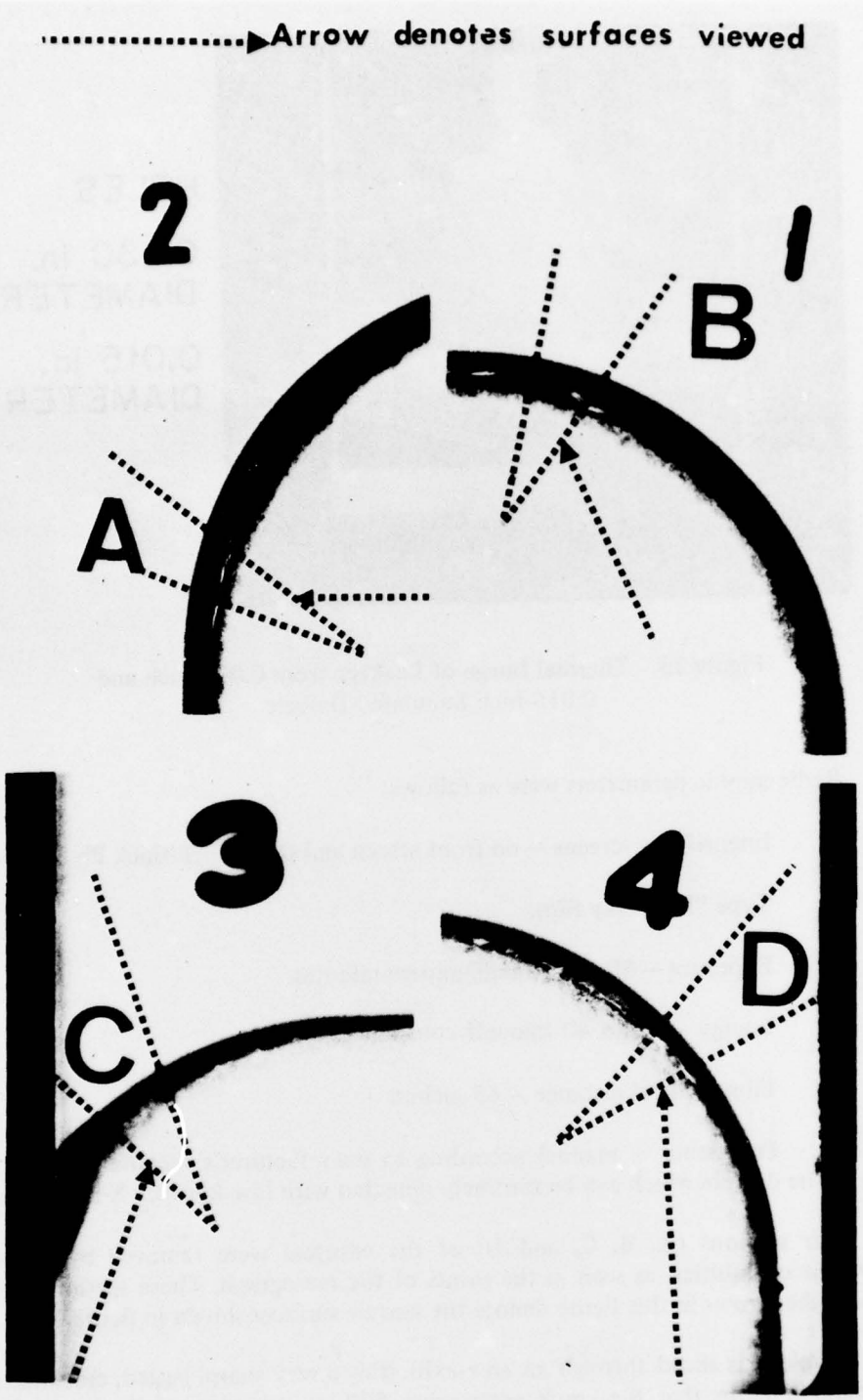

Figure 14. Low Kilovolt X-Ray of Defects in M2 Filter

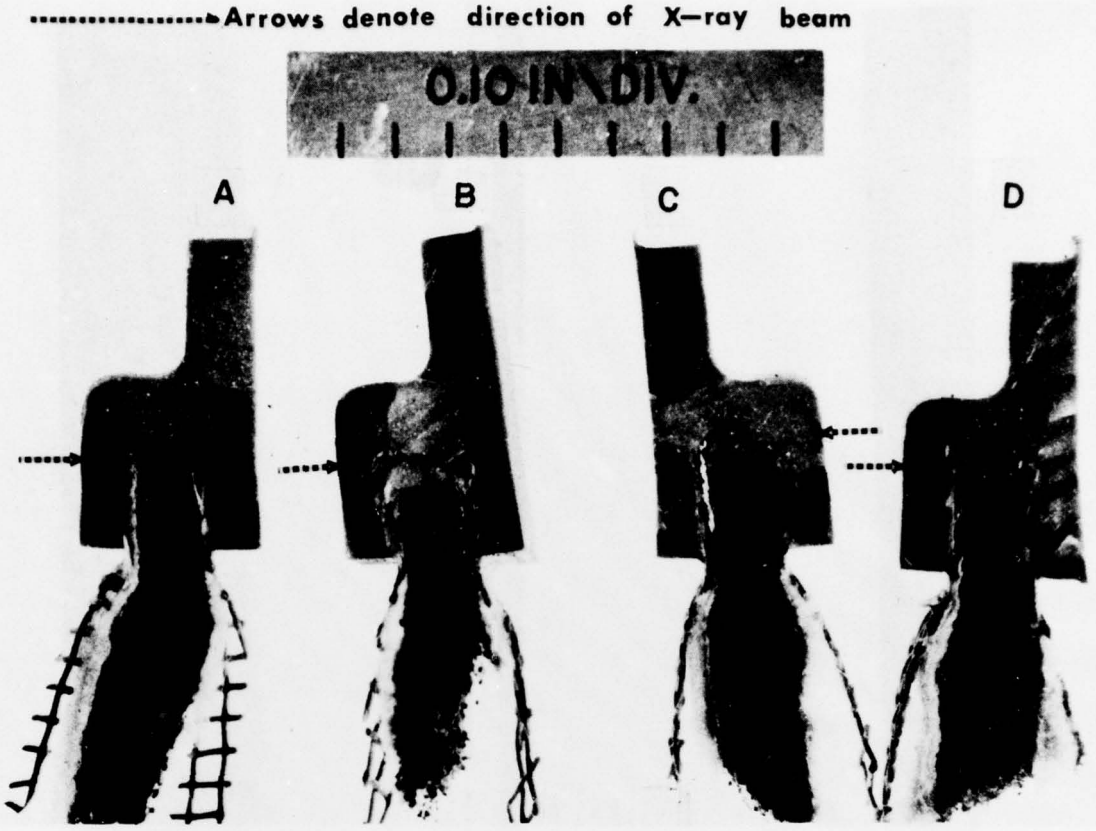

Figure 15. Sample Surfaces Showing Defects in M2 Filter

Sample D showed a wide indication with a very sharp, jagged line near the center on the radiograph. The laminar-type void on the left edgeseal and the crack extending from the right edgeseal are prominent.

C. X-Ray Vidicon.

Using an X-ray vidicon system at Oak Ridge National Laboratory, some filters were monitored for internal flaws on a closed-circuit, 525-lines-per-inch TV screen which also permitted direct still and motion photography.

Figure 16 shows a contact print of a portion of a radiograph of an infant protector filter selected for study. The numbers 8, 9, 10 . . . 22 denote regions of cracking or voids (light areas) in the edgeseal. Area No. 10 was selected for use in determining the optimum conditions. X-ray energies below 120 kv are unsatisfactory. The brightest image was obtained at 140 kv, 30 ma, with the filter located 5-1/2 inch from the X-ray target; however, geometric unsharpness was rather severe. Better resolution, although the image was not as bright, was obtained using the same X-ray energy and current but increasing the filter-to-X-ray target distance to 10 inches. There is a left-to-right reversal of the monitor screen photos as compared to the contact print. This is because conventional viewing of a radiograph is from the X-ray source side while, with the X-ray sensitive vidicon, viewing is from the detector side of the sample.

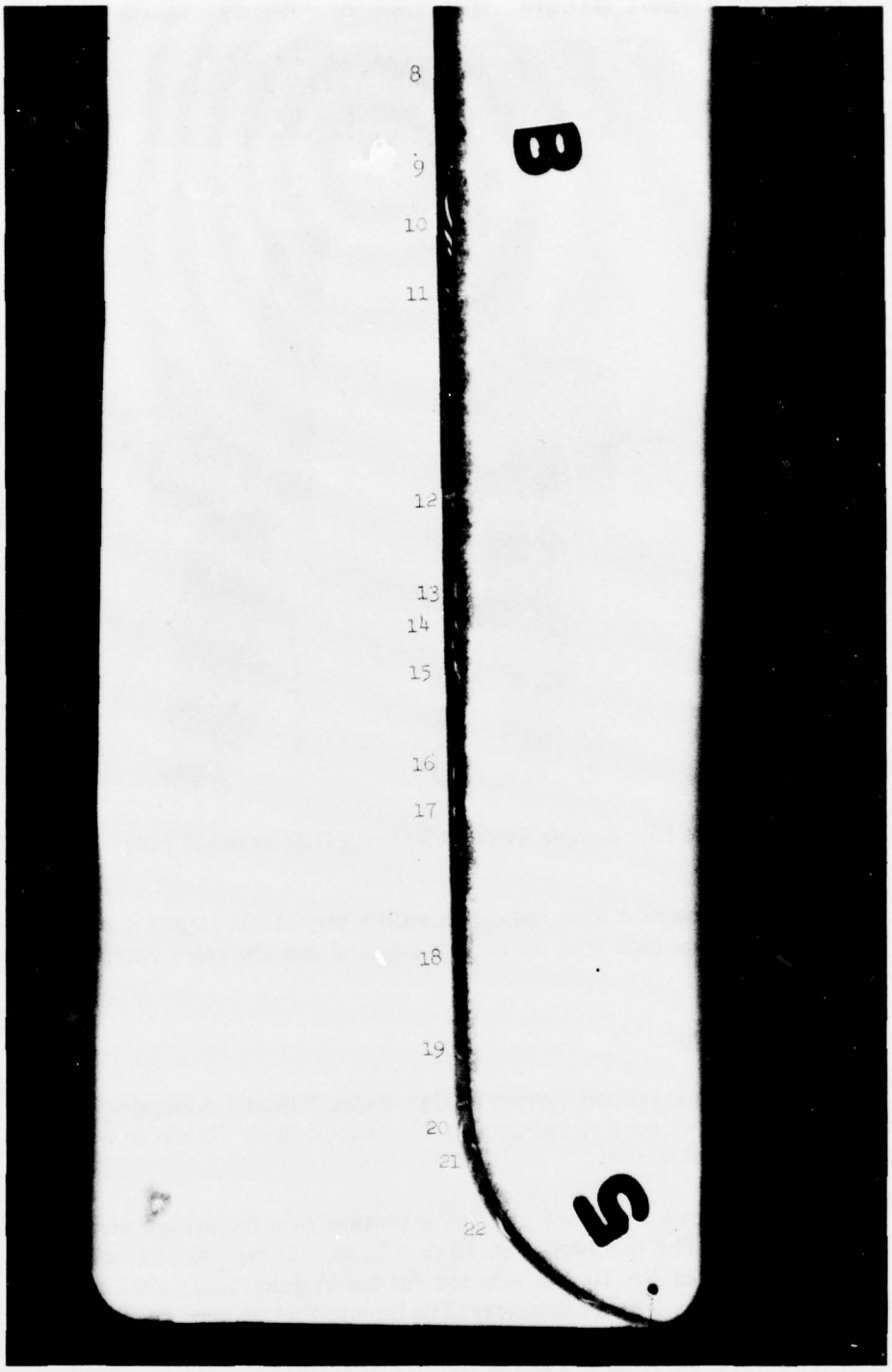

Figure 16. Radiograph of Edgeseal with Numerous Voids

Figure 17 shows two different selected regions (No. 10 and No. 20, respectively) of the filter, as imaged on the monitor screen, using the established optimum conditions of X-ray energy, current distances, and system gain. The white spots seen on the photos are caused by defects in the selenium target of the X-ray sensitive vidicon and would be nonexistent in a new vidicon. The 15 regions denoted in figure 16 were visible on the monitor screen in the static mode.

Dynamic tests were conducted to determine the maximum practical speed that the filter could be moved through the X-ray beam and still permit observation of the filter flaws on the monitor screen. The maximum speed was approximately 52 inches per minute. All 15 regions denoted in figure 16 were visible. In fact, the smaller regions (e.g., No. 18 and No. 20) were more easily seen in this dynamic mode than under in the static conditions.

D. Radiation Gauging.

In this study, gauging was used primarily on the M2 filter panel, using radioactive iodine-125 as a source. Figure 18 shows a print of an X-radiograph of a section from one of the defective filters with significant channel-type voids occurring in the thickest portion of the edgeseal. On the outer surfaces, this area appeared to be defect free; however, destructive sectioning of the filter showed that, in addition to channeling, there was a lack of bonding between those surfaces of the padding and the edgeseal which were in contact. The extent (depth) of the void at the arrow in figure 18 was found to be 29% of the edgeseal thickness at that location. A stripchart recording of the section of filter is shown in figure 19 which is representative of numerous scans ran. Here, a specimen scan speed of 0.025 inch per second was chosen to match the chart speed giving the recorder signature a one-to-one span ratio with defects in the filter. An arbitrary scale intensity gives the relative degree of attenuation of edgeseal material, with the more extensive defects represented by greater amplitudes. The intensity of radiation, incident upon the scintillator, is increased toward the left of the chart. The dips shown near both the beginning and end of the scan are signatures of lead foil markers. The arrow in the center of figure 19 shows the scan of the same channel void pointed out by the arrow in figure 18. The large channel 1-1/4 inches above the arrow is very pronounced in both the radiograph positive print and the chart recording.

The iodine-125 source was positioned 4 inches from the detector, and its 35-kv gamma beam was collimated by a 5/64-inch-diameter orifice in a lead plate. Best scan results in radiation gauging were obtained using a calcium fluoride crystal with a lightproof cover of 1.25-mil aluminized Mylar. Since the $CaF_2(Eu)$ crystal is nonhydroscopic, it can be used without the waterproof seals required for sodium iodide scintillators which significantly attenuate low-energy radiation.

Real-time scanning was used in inspecting each of the three zones of the M2 filter separately. Comparable results were obtained at the maximum dynamic speed of 4.75 inches per minute which was limited by the synchronous, motor-driven specimen platform. Scan results using americium-241 as a source were acceptable but lacked the latitude obtained with iodine-125. Results using a 10 mCi strontium-yttrium-90 source, a 2.2-Mev beta emitter, were considered poor, especially in the area where most of the defects occurred in the M2 filter. The thickness of edgeseal in those areas approached the limit for beta particle transmission. There was also appreciable interference from high-energy gamma associated with beta decay which could not be successfully shielded out.

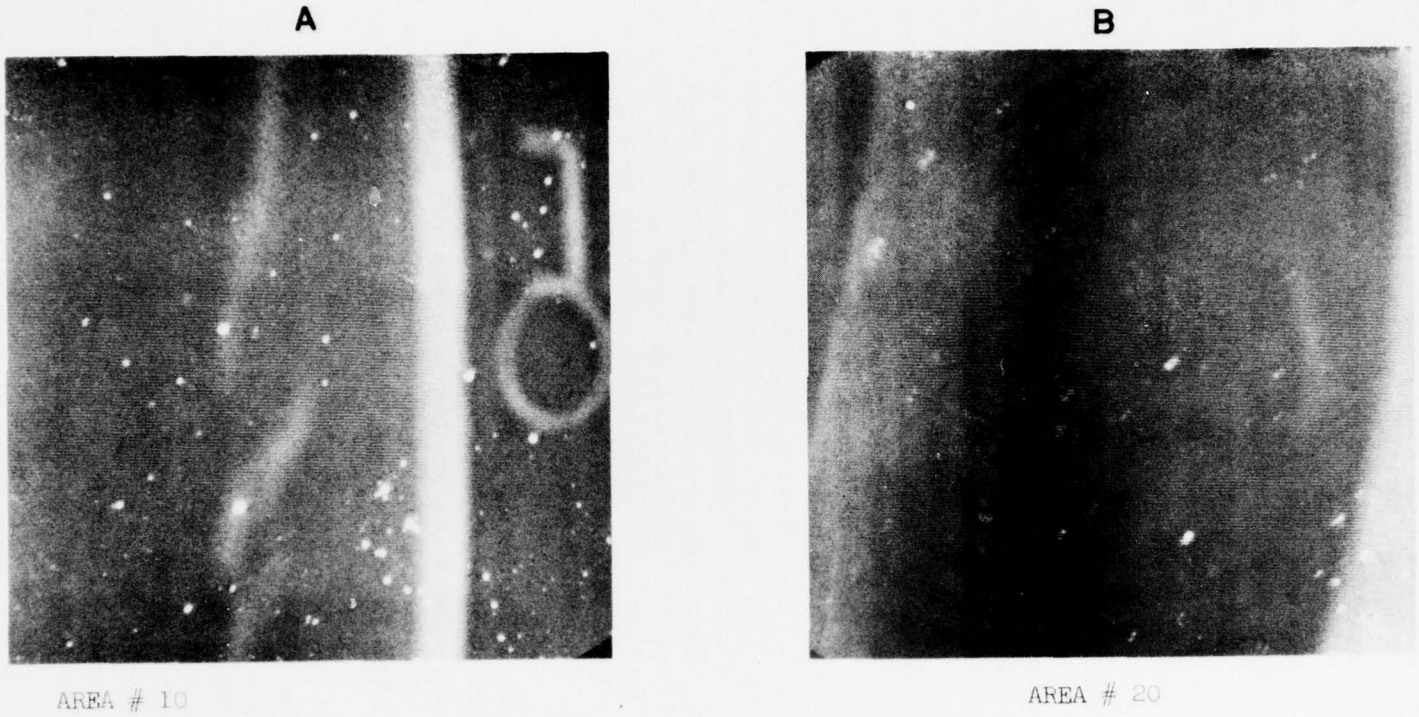

Figure 17. Selected Regions of Defective Filter as Seen on Vidicon TV Monitor

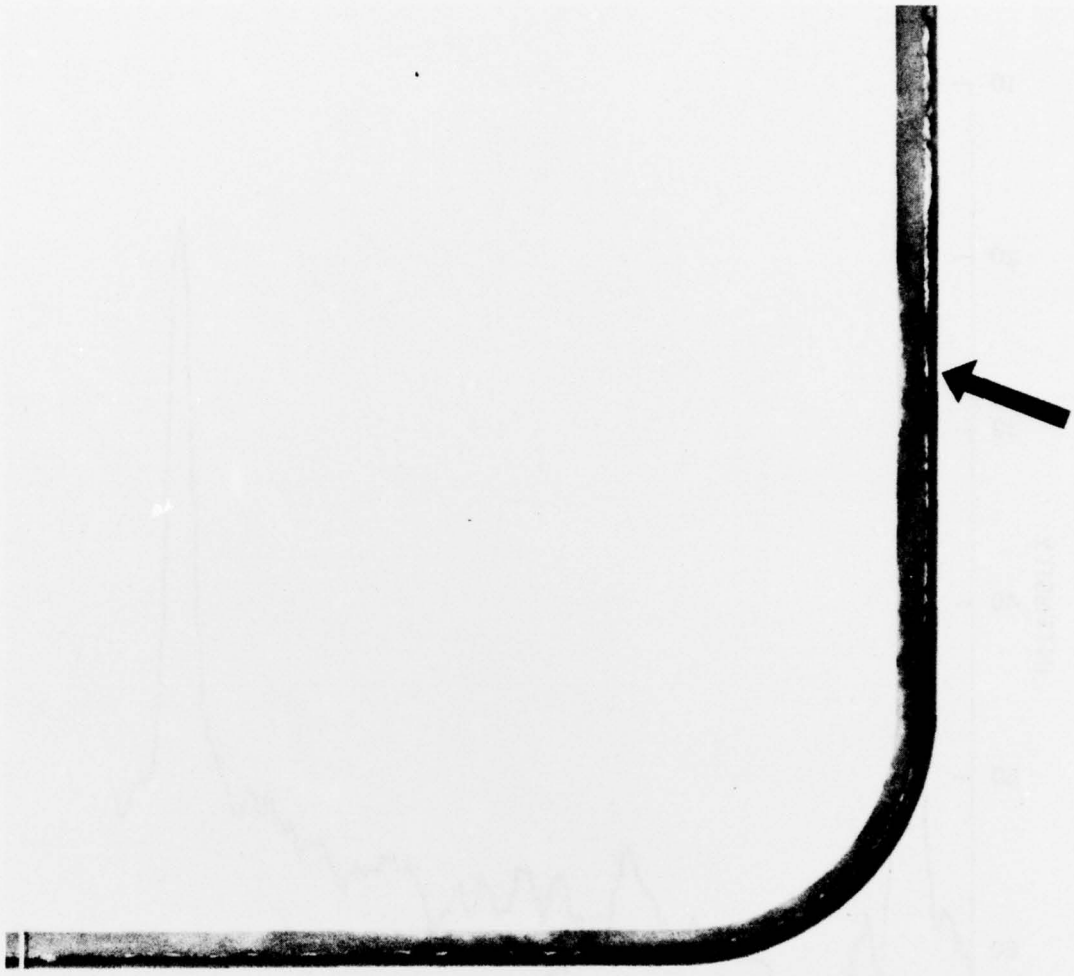

Figure 18. Radiograph of Edgeseal in M2 Filter
Used in Radiation Gauging

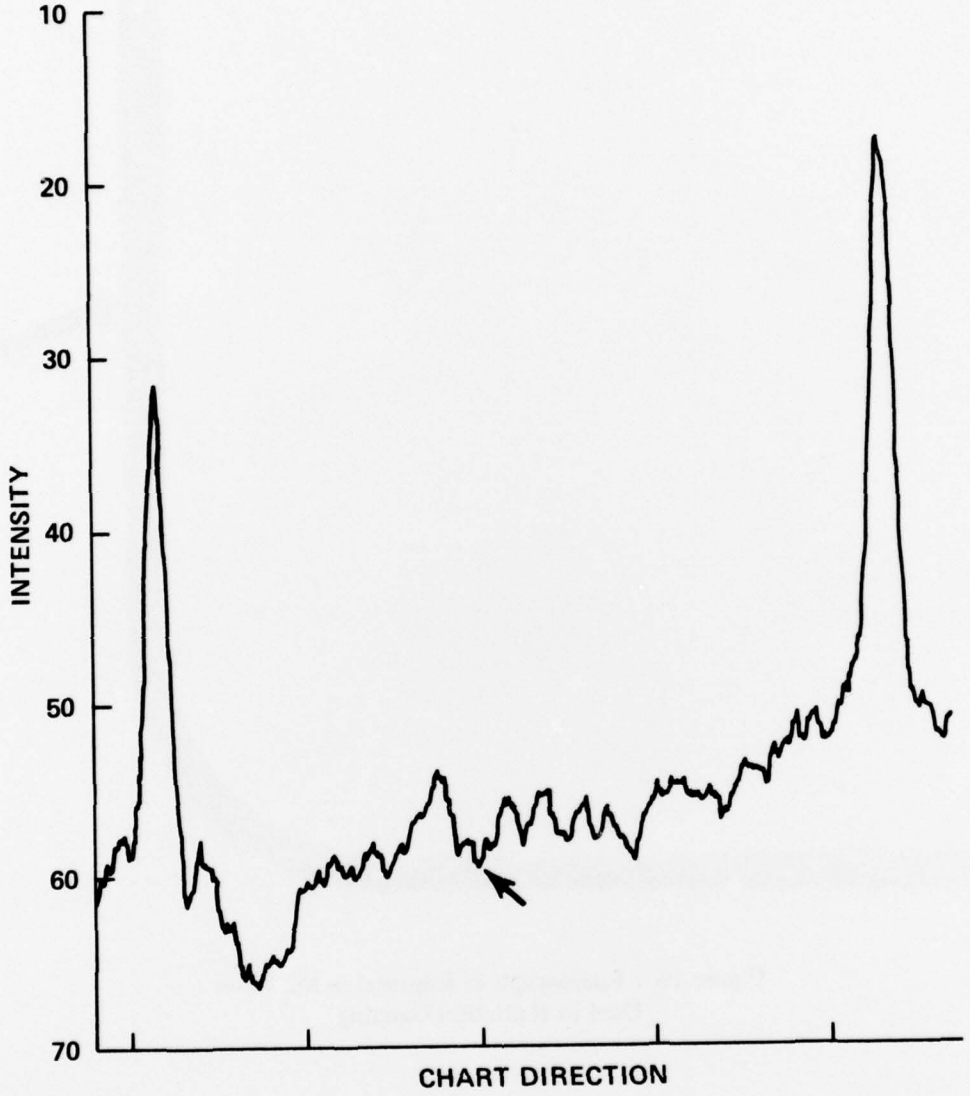

Figure 19. Stripchart Recording of Radiation Gauging of M2 Filter Edgeseal

IV. CONCLUSION.

Protective filter elements can be inspected nondestructively by several proven techniques. Thermal imaging, using infrared devices, was successfully employed to detect some of the internal flaws in the M13A2 filter. Low kilovolt X-radiography revealed most of the defects found in the two types of filters studied in this project. Manual radiography remains available as an aid in questionable cases.

By using the X-ray vidicon, a variety of combinations permitted high-speed inspection. Real-time static, in-motion, or taped examination of defects could be accomplished by automated devices. Radiation gauging also proved successful. It is the least expensive of the nondestructive testing methods considered in this study.

DISTRIBUTION LIST FOR ARCSL-TR-77022

Names	Copies
CHEMICAL SYSTEMS LABORATORY	
OFFICE OF THE DIRECTOR Attn: DRDAR-CLG	1
SAFETY OFFICE Attn: DRDAR-CLF	1
PLANS & PROGRAMS OFFICE Attn: DRDAR-CLR	4
AUTHOR'S COPIES: Chemical Systems Division	100
DEVELOPMENTAL SUPPORT DIVISION Attn: DRDAR-CLJ-I	4
DEPARTMENT OF DEFENSE	
Administrator Defense Documentation Center Attn: Accessions Division Cameron Station Alexandria, VA 22314	12
US ARMY TEST & EVALUATION COMMAND	
Record Copy CDR, APG Attn: STEAP-AD-R/RHA APG-Edgewood Area, Bldg E5179	1
CDR, APG Attn: STEAP-TL APG-Aberdeen Area	1